AN IMPLICIT PROCEDURE FOR THE EULER EQUATIONS
WITH CHEMICAL TERMS

ICAS-94-10.3.2

P. G. SPAZZINI*

Department of Aerospace Engineering, Politecnico di Torino
Corso Duca degli Abruzzi, 24 - I-10129 Torino, Italy

Abstract

Nowadays hypersonic flows are deeply studied because of their importance in perspective. After a phase in which solely pure fluid dynamics at very high speeds was studied, high temperature effects are now starting to be taken into account. It is then important to extend existing computational methods to these phenomena.

In the present work, a time-marching finite volume method is employed for the computation of 2D nonviscous flows with chemical and vibrational activity effects; air is modeled by a 5-species model.

For efficiency purposes, implicit methods should be used; a method belonging to this class is presented here along with some results showing the improvements in efficiency it allows.

1 Introduction

Amongst modern research topics, large interest is being paid to Hypersonic CFD as many long-term projects for high-speed aircraft or re-entry vehicles are being evaluated. Meanwhile, experiments in this field are difficult and expensive to be carried on; CFD becomes thus an useful tool not only for the project design but also for the experiment design itself.

But, what actually *is* an hypersonic flow? This term usually indicates a supersonic flow field in which it is no more possible to neglect high temperature effects, namely a flow field in which the following phenomena show up:

- Vibrational excitation of polyatomic molecules

- Dissociation of polyatomic molecules

- Electronic excitation of all the mixture components, up to ionization

Translational and rotational degrees of freedom are implicitly assumed to be fully excited and in equilibrium at any temperature; this is not a limitative assumption as translational degrees of freedom are already excited immediately after the absolute zero and rotational characteristic temperatures are, with a few exceptions [7], extremely low, while relaxation of these degrees of freedom requires no more than one collision.

It is clear that there is no sharp border line between supersonic and hypersonic flows, as the appearance of these effects is smooth and starts at different Mach numbers depending on the freestream conditions and on the scale lenght of the considered body; anyway, for Mach numbers lower than 3, the flow is in general not hypersonic, while for Mach numbers higher than 5 it usually is.

In the present work, electronic phenomena were not considered, as they show up for temperatures ($\Leftrightarrow$ speeds) much higher than the other effects. In the perspective of a gradual approach, it was then decided to neglect them.

When air dissociates, a mixture composed by a large number of species develops; but many of these components are present in extremely low concentrations, so that they can be neglected. As is done in much of the literature, it was chosen here to represent the dissociating air by a 5-components mixture. The species considered are O, N, NO, O_2, N_2.

2 The mathematics of hypersonic flows

The hypersonic flow fields can be described by the usual Euler (or Navier-Stokes) equations to which some new equations must be added to take into account high temperature effects. In the most general case, one should add one differential equation for the density of any chemical component, one for the vibrational energy of any component who can run into vibrational excitation (i.e. one for each polyatomic molecule), one for any species encountering electronic excitation and one for the charged species diffusion[1]. Nevertheless, many simplifications can be done. First of all, as already mentioned, phenomena involving electrons will

---

*Graduate Student with Politecnico di Torino and von Karman Institute, presently at Politecnico di Torino

[1]Remark that electrons and ions are not cited in this list: they are considered among the chemical species.

not be considered in the present work; moreover, the density of the mixture can be simply obtained as the sum of the densities of the components, so that either the equation for the mixture density (i.e. the continuity equation) or one of the component equations can be dropped out. In the present work it was decided to keep the continuity equation because of the numerical scheme employed (see sec.3). If we suppose that the diffusion of the chemical species is neglectable[2], it is possible to impose the local conservation of the atoms of one kind, which allows to obtain the concentration of molecular oxygen and nitrogen from algebraic equations, so that we can drop one more differential equation. In conclusion, the whole chemical behaviour of the system can be described by just three differential equations. The vibrational behaviour of the system with our model should also be described by three equations as we have three polyatomic species; though, it was shown that the vibrational relaxation time of the NO is always at least one order of magnitude lower than the other two; it makes sense, thus, to assume that the nitrogen monoxide is always in a condition of vibrational equilibrium, so its vibrational energy can be obtained by an algebraic evaluation.

The general form of the differential equations for the evolution of the chemical species is an equation for the *concentration* of the species:

$$(\rho y_i)_t + \text{div}(\vec{V}\rho y_i) = \omega_i \qquad (1)$$

where ρ is the density of the mixture, y_i is the concentration of the species i, $\vec{V}$ the velocity vector and ω_i the production of the species i (in $\frac{\text{kg}}{\text{m}^3\text{s}}$). We can rewrite this equation as an evolution equation for the species density just by developing the terms under differential operators:

$$(\rho_i)_t + \text{div}(\vec{V}\rho_i) = \omega_i \qquad (2)$$

The equations for the vibrational energy have the following form:

$$(\rho_i e_i^v)_t + \text{div}(\vec{V}\rho_i e_i^v) = \omega_i^v \qquad (3)$$

where e_i^v is the vibrational energy per unit volume of the species i. This equation can also be given the alternate form:

$$(\rho e_i^v)_t + \text{div}(\vec{V}\rho e_i^v) = \omega_i^{v\,\prime} \qquad (4)$$

This expression is to be preferred to the former one as it allows to avoid the numerical problems that may show up in zones where the concentration of the species i is close to zero[2].

Reducing to 2D and expanding, the high temperature effects can be computed by the following set of

---

[2]The present work deals only with inviscid cases, for which diffusion is rigourosly zero.

differential equations:

$$\begin{cases} \rho_{O_t} + (u\rho_O)_x + (v\rho_O)_y = \omega_O \\ \rho_{N_t} + (u\rho_N)_x + (v\rho_N)_y = \omega_N \\ \rho_{NO_t} + (u\rho_{NO})_x + (v\rho_{NO})_y = \omega_{NO} \\ (\rho e_{O_2}^v)_t + (\rho u e_{O_2}^v)_x + (\rho v e_{O_2}^v)_y = \omega_{O_2}^v \\ (\rho e_{N_2}^v)_t + (\rho u e_{N_2}^v)_x + (\rho v e_{N_2}^v)_y = \omega_{N_2}^v \end{cases} \qquad (5)$$

Hypersonic flows introduce new phenomena into the motion field; thus, it is necessary to add more similitude parameters into the system. These parameters have been identified in the Damköhler numbers, which are defined as follows:

$$\mathcal{D} = \frac{\tau_{FD}}{\tau_{KV,i}}$$

where τ_{FD} represents a characteristic time of the fluid dynamics (e.g. $\tau_{FD} = \frac{L}{V_\infty}$, L is a characteristic body dimension and V_∞ is the freestream velocity) and τ_{KV} is a characteristic time of the high temperature effects, e.g. the relaxation time of one of the chemical reactions. Observe that any one of the high temperature effects brings a Damköhler number, and that these numbers can be very different from each other. Another important remark is that the Damköhler numbers vary inside the motion field. In the present work, it was decided to typicize the different testcases with a *freestream Damköhler number* ($\mathcal{D}_\infty$), defined as follows: the fluid dynamics time is computed as previously described; for the chemical time, remark that the Jacobian of the source vector (matrix $Z/\mathcal{S}$ in sec. 3.3) has the dimensions of [s^{-1}]. It is then straightforward to choose the inverse of a number connected to this matrix as the reference chemical time. One possible choice for this number is the determinant to the power $\frac{1}{\text{rank of the Jacobian}}$, and this was retained in the present work; another possibility could be the maximum eigenvalue, and so on. The choice preferred here is such that it will bring a value for $\mathcal{D}_\infty$ which is a sort of weighted average. One more decision still has to be taken: in which conditions to compute the Jacobian. An appropriate choice appears to the author to do this computation in the freestream total conditions, i.e.: absence of O, N and NO, absence of vibrational energy, total density, total pressure, total temperature, zero velocity.

3 The numerical method

In the present work, two dimensional chemically reacting flows are computed by a finite volume time marching method. The code implementing this method is an evolution of a conical code for perfect gases developed at von Karman Institute [9, 5, 10].

3.1 Fluxes Evaluation

The flux computation is performed by a Van Leer flux vector splitter adapted to high temperature flows

as described in [3]. The only difference is in that, instead of considering four evolution equations for the chemical species and neglecting the continuity equation, three evolution equations for the species were employed and the continuity equation was kept. As will be more clear from section 3.3, this helped in optimizing the efficiency of the method. Moreover, the equations were reordered so as to have all the high temperature ones grouped together. The splitting structure then reads:

$$F^\pm = f_m^\pm \begin{pmatrix} \rho_O/\rho \\ \rho_N/\rho \\ \rho_{NO}/\rho \\ e_{O2}^v \\ e_{N2}^v \\ 1 \\ [(\tilde\gamma-1)\,u \pm 2a\cdot n_x]/\tilde\gamma \\ [(\tilde\gamma-1)\,v \pm 2a\cdot n_y]/\tilde\gamma \\ f_e^\pm \end{pmatrix} \qquad (6)$$

where

$$f_m^\pm = \pm\rho a \left(\frac{\pm M_n + 1}{2} \right)^2$$

and

$$f_e^\pm = \frac{\left[(\tilde\gamma-1)\sqrt{u^2+v^2} \pm 2a\right]^2}{2(\tilde\gamma^2-1)} + \sum \frac{\rho_i}{\rho}\left(e_i^v + h_i^0\right)$$

3.2 Source terms

Many different chemical and vibrational energy source term models were implemented into the code, but in the present work only the Park model [6] for chemistry has been used.

3.3 Time integration: the LUSKE[3]scheme

The implicit time integration procedure developed by the author is typicized by the following features:

- Full coupling between high temperature effects equations

- Weakened coupling between the fluid dynamics equations

- Decoupling between the high temperature and the fluid dynamics sections during the time integration

Let's now analyze in detail the different sections of the time integration.

---

[3]Lower-Upper Scheme for (K)emical Evolution.

Fluid dynamics

For this section a Jameson and Yoon LU-SSOR procedure is employed; the principles of the method, fully described in [4, 11], will hereafter be quickly recalled. Consider the 2-D Euler equations in vector form:

$$\mathbf{W}_t + \mathbf{F}_x + \mathbf{G}_y = 0 \qquad (7)$$

where

$$\mathbf{W} = (\rho, \rho u, \rho v, \rho E)^{\mathrm{T}}$$
$$\mathbf{F} = u(\rho, \rho u + p, \rho v, \rho H)^{\mathrm{T}}$$
$$\mathbf{G} = v(\rho, \rho u, \rho v + p, \rho H)^{\mathrm{T}}$$

and the most general form for a 1-stage time integration scheme:

$$S_{i,j}\frac{\Delta\mathbf{W}_{i,j}}{\Delta t} + \eta\sum_{\beta=1}^{4}(\mathbf{F}_{\mathrm{NUM}}\cdot\mathbf{n}\Delta s)_\beta^{n+1} +$$

$$+(1-\eta)\sum_{\beta=1}^{4}(\mathbf{F}_{\mathrm{NUM}}\cdot\mathbf{n}\Delta s)_\beta^{n} = 0 \qquad (8)$$

Here, $\Delta\mathbf{W}_{i,j}$ is the time variation of the solution at the cell center i,j and η is a parameter weighting the numerical flux between the two time levels n and $n+1$: $\eta = 0$ is a fully explicit scheme and $\eta = 1$ a fully implicit one; S is the cell surface and Δs_β are the cell border lenghts (see fig. 1). If we introduce the inviscid
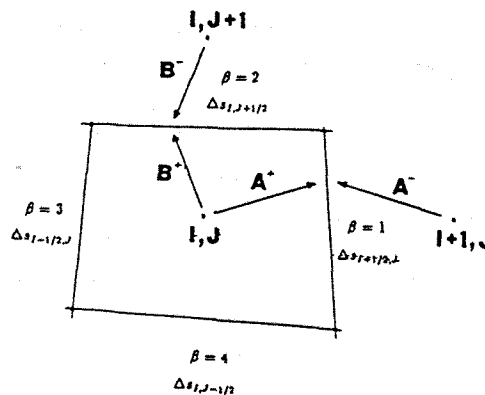

Figure 1: Computational cell and splitting of the Jacobians

flux Jacobians and linearize, (8) becomes:

$$\frac{(S\Delta\mathbf{W})_{i,j}}{\Delta t} + \eta\sum_{\beta=1}^{4}[(An_x + Bn_y)\Delta s]_\beta^n \,\Delta\mathbf{W}_\beta = \mathcal{R}_{i,j}^n$$

$$(9)$$

where A and B are the flux Jacobians in the coordinate directions and $\mathcal{R}_{i,j}^n$ is the flux balance at time level n for the cell i,j. It is useful to indicate with $\hat{A}$ and $\hat{B}$, respectively, the Jacobians of the fluxes in the direction normal to the cell faces $\beta = 1, 3$ and $\beta = 2, 4$:

$$\hat{A} = (An_x + Bny)_{\beta=1,3}$$

$$\hat{B} = (An_x + Bny)_{\beta=2,4}$$

It is possible to obtain a block triangular form of the implicit operator as follows. First, the contribution of the inviscid flux Jacobians at each cell face is split into a positive and a negative part (see fig. 1):

$$(\hat{A}\Delta\mathbf{W})_{i+\frac{1}{2},j} = \hat{A}^+_{i,j}\Delta\mathbf{W}_{i,j} + \hat{A}^-_{i+1,j}\Delta\mathbf{W}_{i+1,j}$$

Similar relations hold for the other faces. The Jacobians $\hat{A}^\pm$, $\hat{B}^\pm$ are constructed so that the positive (negative) matrices have non negative (non positive) eigenvalues. A better conditioned implicit operator is obtained by increasing its diagonal dominance. For that purpose, Yoon and Jameson proposed the following splitting:

$$\hat{A}^\pm = \frac{\hat{A} \pm \gamma_A I}{2} \qquad (10)$$

with

$$\gamma_A = r_A \max(|\lambda_A|)$$

λ_A are the eigenvalues of $\hat{A}$ and r_A is a constant of order 1; similarly for $\hat{B}^\pm$. Furthermore, the computational efficiency of the method can be enhanced by an overrelaxation technique, which is obtained by redefining $\hat{A}^\pm$, $\hat{B}^\pm$ by the insertion of an overrelaxation parameter:

$$\hat{A}^\pm = \chi \frac{\hat{A} \pm \gamma_A I}{2} \qquad (11)$$

Posing now in (9) $\frac{\Delta t}{S_{i,j}} = \vartheta$, multiplying all the terms by ϑ, substituting and reorganizing, we obtain ($\alpha = \eta \cdot \vartheta$):

$$\left[I + \alpha \left(\hat{A}^+_{i,j}\Delta s_1 - \hat{A}^-_{i,j}\Delta s_3 + \hat{B}^+_{i,j}\Delta s_2 + \right.\right.$$
$$\left.\left. - \hat{B}^-_{i,j}\Delta s_4 \right) \right] \Delta\mathbf{W}_{i,j} + \alpha \left(-\hat{A}^+_{i-1,j}\Delta s_3\Delta\mathbf{W}_{i-1,j} + \right.$$
$$\left. - \hat{B}^+_{i,j-1}\Delta s_4\Delta\mathbf{W}_{i,j-1} \right) + \alpha \left(\hat{A}^-_{i+1,j}\Delta s_1\Delta\mathbf{W}_{i+1,j} + \right.$$
$$\left. - \hat{B}^-_{i,j+1}\Delta s_2\Delta\mathbf{W}_{i,j+1} \right) = \vartheta\mathcal{R} \qquad (12)$$

Let N, M^+, M^- be the following matrices:

$$N = I + \alpha \left[\left(\hat{A}^+_{i,j}\Delta s_1 - \hat{A}^-_{i,j}\Delta s_3 \right) \right.$$
$$\left. + \left(\hat{B}^+_{i,j}\Delta s_2 - \hat{B}^-_{i,j}\Delta s_4 \right) \right]$$

$$M^+ = -\hat{A}^+_{i-1,j}\Delta s_3\Delta\mathbf{W}_{i-1,j} - \hat{B}^+_{i,j-1}\Delta s_4\Delta\mathbf{W}_{i,j-1}$$

$$M^- = \hat{A}^-_{i+1,j}\Delta s_1\Delta\mathbf{W}_{i+1,j} - \hat{B}^-_{i,j+1}\Delta s_2\Delta\mathbf{W}_{i,j+1}$$

If the variations of Δs across the cell are neglected and $\Delta\bar{x}$, $\Delta\bar{y}$ are the mean values, N becomes a *scalar* matrix[4]:

$$N = [1 + \alpha (\gamma_A\Delta\bar{y} + \gamma_B\Delta\bar{x})]$$

[4]This terms indicates a diagonal matrix who is the identity matrix multiplied by a scalar.

Hence, equation (12) can be factorized as follows:

$$\left[\left(N + \alpha M^+ \right) N^{-1} \left(N + \alpha M^- \right) \right] \Delta\mathbf{W} = \vartheta\mathcal{R} \qquad (13)$$

so that we can obtain the solution *without any matrix inversions* through the following two-sweep process[5]:

$$\Delta\mathbf{W}^* = N^{-1} \left(\vartheta N\mathcal{R} - \alpha M^+ \right) = \vartheta\mathcal{R} - \alpha N^{-1}M^+$$

$$\Delta\mathbf{W} = N^{-1} \left(\Delta\mathbf{W}^* - \alpha M^- \right)$$

High temperature effects

An hybrid LU procedure is employed in this section. Consider the system of the high temperature effects equations (5); it is obviuosly possible to write it in vector form as follows:

$$\mathbf{W}^a_t + \mathbf{F}^a_x + \mathbf{G}^a_y = \Omega \qquad (14)$$

where

$$\mathbf{W}^a = (\rho_O, \rho_N, \rho_{NO}, \rho e^v_{O2}, \rho e^v_{N2})^{\mathrm{T}}$$
$$\mathbf{F}^a = u(\rho_O, \rho_N, \rho_{NO}, \rho e^v_{O2}, \rho e^v_{N2})^{\mathrm{T}}$$
$$\mathbf{G}^a = v(\rho_O, \rho_N, \rho_{NO}, \rho e^v_{O2}, \rho e^v_{N2})^{\mathrm{T}}$$
$$\Omega = (\omega_O, \omega_N, \omega_{NO}, \omega^v_{O2}, \omega^v_{N2})^{\mathrm{T}}$$

Discretizing and putting in implicit form yields:

$$S_{i,j}\frac{\Delta\mathbf{W}}{\Delta t} + \eta \left[\sum_{\beta=1}^{4} \left(\bar{\mathbf{F}}_{\mathrm{num}} \cdot \mathbf{n}\Delta s \right)_\beta - S_{i,j}\Omega \right]^{n+1} +$$
$$+ (1-\eta) \left[\sum_{\beta=1}^{4} \left(\bar{\mathbf{F}}_{\mathrm{num}} \cdot \mathbf{n}\Delta s \right)_\beta - S_{i,j}\Omega \right]^n = 0 \qquad (15)$$

Observing that $\Omega^{n+1} \sim \Omega^n + \frac{\partial\Omega}{\partial t}\Delta t$, $\frac{\partial\Omega}{\partial t} \sim \frac{\partial\Omega}{\partial\mathbf{W}}\frac{\Delta\mathbf{W}}{\Delta t}$ and thus $\Omega^{n+1} \sim \Omega^n + \frac{\partial\Omega}{\partial\mathbf{W}}\Delta\mathbf{W}$, it is possible to linearize the source term and obtain:

$$S_{i,j}\frac{\Delta\mathbf{W}}{\Delta t} + \eta \left[\sum_{\beta=1}^{4} \left(\frac{\partial\bar{\mathbf{F}}_{\mathrm{num}}}{\partial\mathbf{W}} \cdot \mathbf{n}\Delta s \right)_\beta \Delta\mathbf{W} + \right.$$
$$\left. - S_{i,j}\frac{\partial\Omega}{\partial\mathbf{W}}\Delta\mathbf{W} \right]^{n+1} = \mathcal{R}^n_{i,j} + S_{i,j}\Omega^n \qquad (16)$$

or, posing $\mathcal{R}^n_{i,j} + S_{i,j}\Omega^n = \mathcal{K}^n_{i,j}$:

$$S_{i,j}\frac{\Delta\mathbf{W}}{\Delta t} + \eta \left[\sum_{\beta=1}^{4} \left(\frac{\partial\bar{\mathbf{F}}_{\mathrm{num}}}{\partial\mathbf{W}} \cdot \mathbf{n}\Delta s \right)_\beta \Delta\mathbf{W} + \right.$$
$$\left. - S_{i,j}\frac{\partial\Omega}{\partial\mathbf{W}}\Delta\mathbf{W} \right]^{n+1} = \mathcal{K}^n_{i,j} \qquad (17)$$

[5]Remark that, N being a scalar matrix, the factorization is unique.

Again, we linearize the fluxes and get:

$$\left\{ \frac{S_{i,j}}{\Delta t} I + \eta \sum_{\beta=1}^{4} [(An_x + Bn_y)\,\Delta s]_\beta + \right.$$

$$\left. -\eta S_{i,j} \frac{\partial \Omega}{\partial \mathbf{W}} \right\} \Delta \mathbf{W} = \mathcal{K}_{i,j}^n \qquad (18)$$

or (α, ϑ as previously):

$$\left\{ I + \alpha \sum_{\beta=1}^{4} [(An_x + Bn_y)\,\Delta s]_\beta + \right.$$

$$\left. -\alpha S_{i,j} \frac{\partial \Omega}{\partial \mathbf{W}} \right\} \Delta \mathbf{W} = \vartheta \mathcal{K}_{i,j}^n \qquad (19)$$

As in the case of the LU-SSOR method, we split the contribution of the flux Jacobians at each cell face into a positive and a negative part. Defining $\hat{A}^\pm$, $\hat{B}^\pm$ as in the fluid dynamics section, expanding equation (19) after splitting and reorganizing the terms, we obtain:

$$\left[I + \alpha \left(\hat{A}_{i,j}^+ \Delta s_1 - \hat{A}_{i,j}^- \Delta s_3 + \hat{B}_{i,j}^+ \Delta s_2 - \hat{B}_{i,j}^- \Delta s_4 + \right. \right.$$

$$\left. \left. -S_{i,j} \frac{\partial \Omega}{\partial \mathbf{W}} \right) \right] \Delta \mathbf{W}_{i,j} + \alpha \left(-\hat{A}_{i-1,j}^+ \Delta s_3 \Delta \mathbf{W}_{i-1,j} + \right.$$

$$\left. -\hat{B}_{i,j-1}^+ \Delta s_4 \Delta \mathbf{W}_{i,j-1} \right) + \alpha \left(\hat{A}_{i+1,j}^- \Delta s_1 \Delta \mathbf{W}_{i+1,j} + \right.$$

$$\left. -\hat{B}_{i,j+1}^- \Delta s_2 \Delta \mathbf{W}_{i,j+1} \right) = \vartheta \mathcal{K}_{i,j}^n \qquad (20)$$

If we introduce the following formalism:

$$Z = -S_{i,j} \frac{\partial \Omega}{\partial \mathbf{W}}$$

$$N = \hat{A}_{i,j}^+ \Delta s_1 - \hat{A}_{i,j}^- \Delta s_3 + \hat{B}_{i,j}^+ \Delta s_2 - \hat{B}_{i,j}^- \Delta s_4$$

$$M^+ = -\hat{A}_{i-1,j}^+ \Delta s_3 \Delta \mathbf{W}_{i-1,j} - \hat{B}_{i,j-1}^+ \Delta s_4 \Delta \mathbf{W}_{i,j-1}$$

$$M^- = \hat{A}_{i+1,j}^- \Delta s_1 \Delta \mathbf{W}_{i+1,j} - \hat{B}_{i,j+1}^- \Delta s_2 \Delta \mathbf{W}_{i,j+1}$$

we see that (20) becomes:

$$\left[I + \alpha(N + Z) + \alpha M^+ + \alpha M^- \right] \Delta \mathbf{W} = \vartheta \mathcal{K}_{i,j}^n \quad (21)$$

And finally, imposing $J = I + \alpha(N + Z)$,

$$\left[J + \alpha M^+ + \alpha M^- \right] \Delta \mathbf{W} = \vartheta \mathcal{K}_{i,j}^n \qquad (22)$$

The matrix multiplying vector $\Delta \mathbf{W}$ can be factorized as follows:

$$\left[J + \alpha M^+ + \alpha M^- \right] \sim (J + \alpha M^+) J^{-1} (J + \alpha M^-) \qquad (23)$$

We get then to the lower/upper decomposition that reads[6]:

$$\Delta \mathbf{W}^* = \vartheta \mathcal{K}_{i,j}^n - \alpha J^{-1} M^+$$

$$\Delta \mathbf{W} = J^{-1} \left(\Delta \mathbf{W}^* - \alpha M^+ \right)$$

---

[6]Remark that matrix J is *not* a scalar matrix, so that there is another way of performing the decomposition that, in principle, is not identical to the present one. Though, that version was tested and was observed to bring no noticeable differences neither in results nor in performances. Then it was decided to implement the present form mainly for reasons of coherence with the fluid dynamics section.

3.4 Peculiarities and fine-tuning

The code offers the opportunity to freeze the matrices employed in the computations for some timesteps. This is important because the evaluation of these matrices, and in particular of the ones used for the high temperature section, is extremely expensive. Unfortunately, some test cases do not sustain this trick, thus imposing a step-by-step evaluation of the Jacobians.

In many cases, the high temperature shock is so strong that, if inserted steeply, it can cause the code to fail. Then, it was made possible to relax the insertion of high temperature effects over N steps. This is obtained by multiplying the source terms by a factor whose value is $\left(\frac{399 \times (1 - \text{STEP})}{400 \times (1 - N)} + \frac{1}{400} \right)^{4.8}$ if STEP $<$ N, 1 if STEP $\geq$ N.

****

The method just described allows a cost effective solution of the full system, as will be shown in section 4. Remark that, would four species evolution equations be used, the dimension of the matrices to be inverted for the LU high temperature section would increase to 6×6, which would have a non-neglectable effect on the CPU time required for one iteration.

If the method was applied to more complex gas models, the size of the matrices to be inverted would increase with the numbers of equations and the CPU time would then rapidly grow to unacceptable levels. In such cases, it appears then a proper workpath to break the set of high temperature effects equations into two parts, the first, to be solved with the present method, including the "most critical" ones, which will be the ones with lower relaxation times in order to skip stiffness problems (see section 4), and the second, including the remaining equations, to be solved with less time-consuming methods.

4   Results and discussion

Two test cases will be presented hereafter. In both testcases only chemical activity effects were considered. From the numerical viewpoint, this means only that the last two rows and columns in the matrix J (see 3.3) will be 0 except for the diagonal terms which will be nonzero.

All the computations were performed on a DEC 3000/500 *Alpha* computer.

Testcase 1: Diverging Nozzle

This is a quasi 1-D testcase. It was run as a preliminary testcase and to underline the peculiarities of the interaction between fluid dynamics and non equilibrium phenomena. A 12 × 51 cylindrical grid was employed (fig. 2). Remark that, given the geometry of

the flow, only one computational cell in the transversal direction would have been sufficient. The opening angle of the nozzle is 45^0 and its lenght twice the radius of the inlet section. For the typical lenght required in the computation of the Damköhler number, the nozzle lenght is taken.
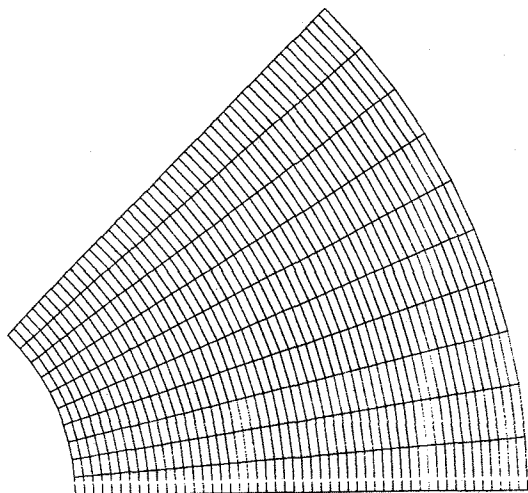

Figure 2: Computational grid for testcase 1

The inlet conditions are: $M_\infty=12.0$, $T^0=7450$ K and $p^0=7.22 \cdot 10^5$ Pa. The imposed outlet static pressure is $p_{out}=5.67 \cdot 10^2$ Pa, causing the shock to be positioned at 30% of the nozzle in the absence of high temperature effects.

The baseline lenght considered was of 2.5 cm (testcase 1.1), corresponding to a freestream Damköhler number of about 150. The lenght was then increased by multiples of 10.

Figs. 3 to 7 show the distribution of the O, N and NO concentrations on the nozzle axis for some significant testcases.

Observe the evolution of these quantities from the frozen values of fig. 3 through the different nonequilibrium situations to the equilibrium values of fig. 7. The frozen conditions are put in evidence by the fact that the concentration of chemical species is very close to the freestream conditions. This happens because the fluid dynamics characteristic time (permanence time) is very low, so that the chemical reactions have no time to develop within the nozzle. This situation is typical of low Damköhler number flows. On the other side, we have equilibrium situations when the fluid dynamics time is much larger than the activity characteristic time (high Damköhler number) so that the chemical reactions adapt to the evolution of the environment very quickly. In these cases the change from freestream conditions to full dissociation is obtained within a few cells. Remark the typical peak in the NO concentration distributions. This configuration appears because in the initial zone behind the shock there is still a high percentage of molecular oxygen, that can be involved

in an exchange reaction with molecular nitrogen which brings to a nitric oxide production larger than the one caused by the association reaction involving atomic oxygen and nitrogen. When, later, O_2 concentration becomes low, the NO concentration of equilibrium imposed by the latter reaction is reached.

Table 1 presents, along with the freestream Damköhler number, some quantities that can help in a quantitative evaluation of the distance from equilibrium: the position of the [NO] peak,the maximum concentration of atomic oxygen and the outlet temperature. It can be observed that changes in these quantities are very strong in the first cases but become neglectable in the last ones, indicating that equilibrium is closely approximated.

T.C.	$\mathcal{D}_\infty$	[NO] peak position	max. [O]	max. T
1.1	150	Outside	.0558	7219
1.2	1500	Outside	.1232	6853
1.3	15000	57%	.1737	6388
1.4	150000	37%	.2140	5316
1.5	1.5E6	35%	.2263	4566
1.6	1.5E7	35%	.2265	3977
1.7	1.5E8	35%	.2265	3604
1.8	1.5E9	33%	.2265	3545

Table 1: Quantitative results for testcase 1

Remark that the peak of NO is steady from testcases 1.5 to 1.7 and then moves in testcase 1.8. Moreover, in the last cases the peak value reduces, while one would expect a constant peak and a self similar shape in all the cases. This happens because the number of computational points is constant for all the testcases, so that in the last ones the NO evolution amplitude shrinks to just one cell and we have a loss of resolution.
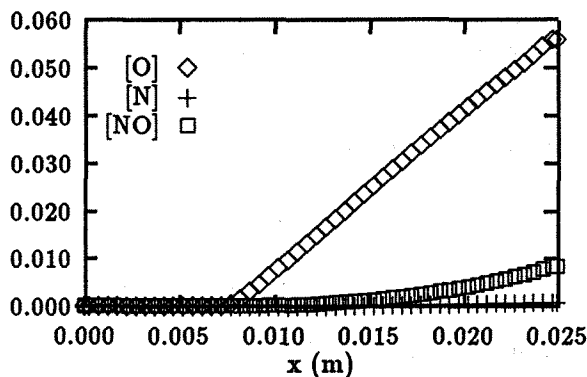

Figure 3: Species concentration, testcase 1.1

It is interesting to observe that the code based on the time integration scheme proposed in the present report allows full computation over a very wide range
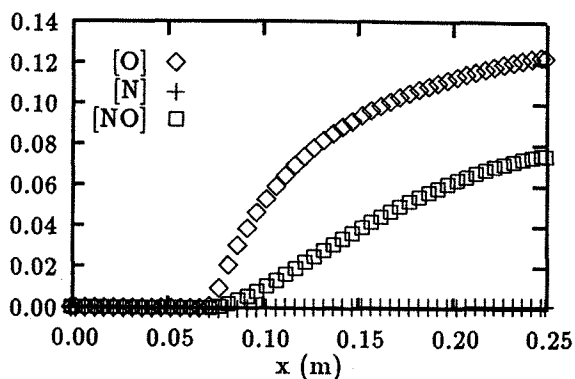
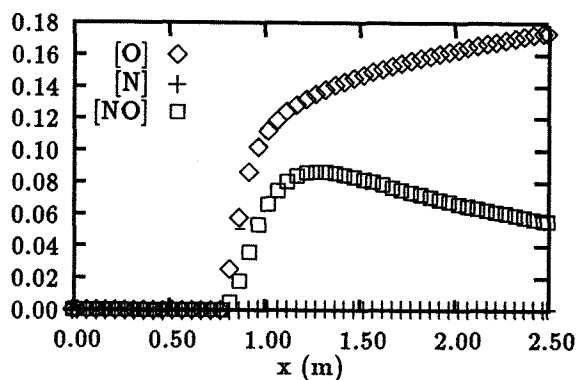Figure 4: Species concentration, testcase 1.2

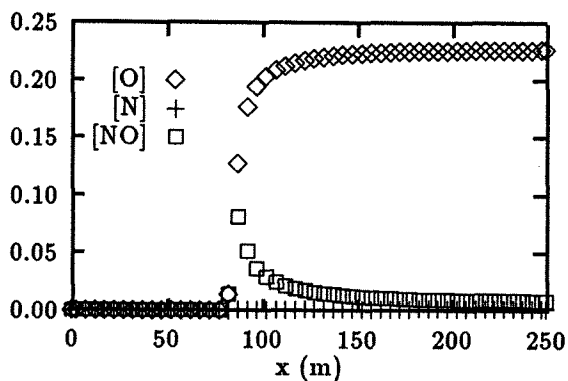Figure 5: Species concentration, testcase 1.3

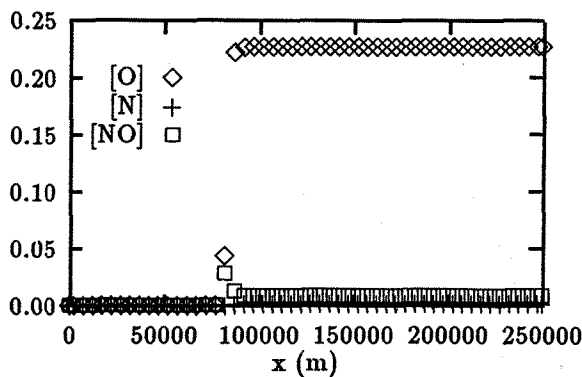Figure 6: Species concentration, testcase 1.5

Figure 7: Species concentration, testcase 1.8

of Damköhler numbers. On the contrary, all previous works reported of numerical instabilities that inhibit other schemes from computing near-equilibrium values with nonequilibrium methods. As a consequence, specific computations are usually required for equilibrium flows. This implies of course a problem much heavier than the simple requirement of two different codes, as the range to which a particular testcase belongs is often unknown *a priori* . The wide efficacy of the present scheme is then to be considered a major improvement; the cause of this efficacy is presently being studied and will be discussed more deeply in a follow-on article. Another remark to be done is that equilibrium was *not* actually reached, as for extremely large values of $\mathcal{D}_\infty$ numerical instability was observed also on this code; this is correct as it is theoretically impossible to compute a fully equilibrium flow with nonequilibrium methods[7]. What actually happens is that the present method allows to approach much further the equilibrium situation before giving up. Anyway, the difference is so small that, from a practical point of view, it can be stated that the equilibrium is reached.

Testcase 2: Blunt Body

The body considered here is a half cylinder followed by a slab.

This is a fully 2-D testcase and has been performed for a more thorough testing of the method. The testcase is quite hard as it implies a bow shock of different strenght depending on the position around the body and a strong expansion interacting with the shock itself. The chemical evolution is therefore much more complex than in the previous testcase; indeed, temperature faces a sharp increase (at the bow shock location) followed by a fluid dynamics driven reduction (expansion) which interacts with the reduction driven by the

---

[7]Indeed, a fully equilibrium flow is just an idealization as the full relaxation requires an infinite time to be obtained.

chemical reactions themselves. Again, many testcases were run with the same geometrical configuration, but with a scale factor of 10 between a case and the following. Test conditions were the following: freestream mach number 12.2, freestream static pressure 43 Pa, freestream static temperature 266 K, no incidence. Table 2 shows the body dimensions for the various subcases run along with some quantitative results displaying once more the capability of the scheme to handle problems characterized by a wide field of Damköhler numbers. The radius of the bodies is in meters, the shock position is the distance of the bow shock from the body nose expressed as a fraction of the body radius. For comparison, a pure fluid dynamics and an equilibrium computation were also performed on the same geometry (testcases 2.0 and 2.11, respectively)

T.C.	Body radius	$\mathcal{D}_\infty$	Shock position	max. T
2.0	-	-	0.396	8140
2.1	0.005	341.	0.35	7878
2.2	0.05	3.41E3	0.29	7555
2.3	0.5	34.1E3	0.249	6860
2.4	5.	341E3	0.224	5716
2.5	50.	3.41E6	0.215	4784
2.6	500.	34.1E6	0.212	4306
2.7	5.E3	341.E6	0.2116	4129
2.8	50.E3	3.41E9	0.2114	4129
2.9	500.E3	34.1E9	0.2114	4129
2.10	5.E6	341.E9	0.2114	4129
2.11	-	-	0.2114	4129

Table 2: Quantitative results for testcase 2

It is evident that the cases with very small body dimensions are very close to the pure fluid dynamics case (frozen cases) while in the upper end of the computational field changes between two testcases become neglectable (flow is tending to equilibrium).

Observe that theoretical analysis suggests that the maximum temperature should always be almost the same as in the equilibrium computation if chemical reactions are considered because in the stagnation point equilibrium conditions must be reached [8]. But this is connected to phenomena happening to a much smaller scale and it is not surprising that the code was not able to catch this behaviour. Presently the only known method to observe stagnation point equilibrium is a data postprocessing method based on integration along the computed streamlines.

Figs. 8 and 9 present the results of these testcases in graphical form by the O concentration fields; fig. 10 presents a comparison of the pressure fields for test cases 2.0, 2.3, 2.9 and 2.11. The shift in the shock location shown in table 2 is quite evident. This shift appears as the introduction of chemical reactions reduces the amount of energy available for the fluid dynamics
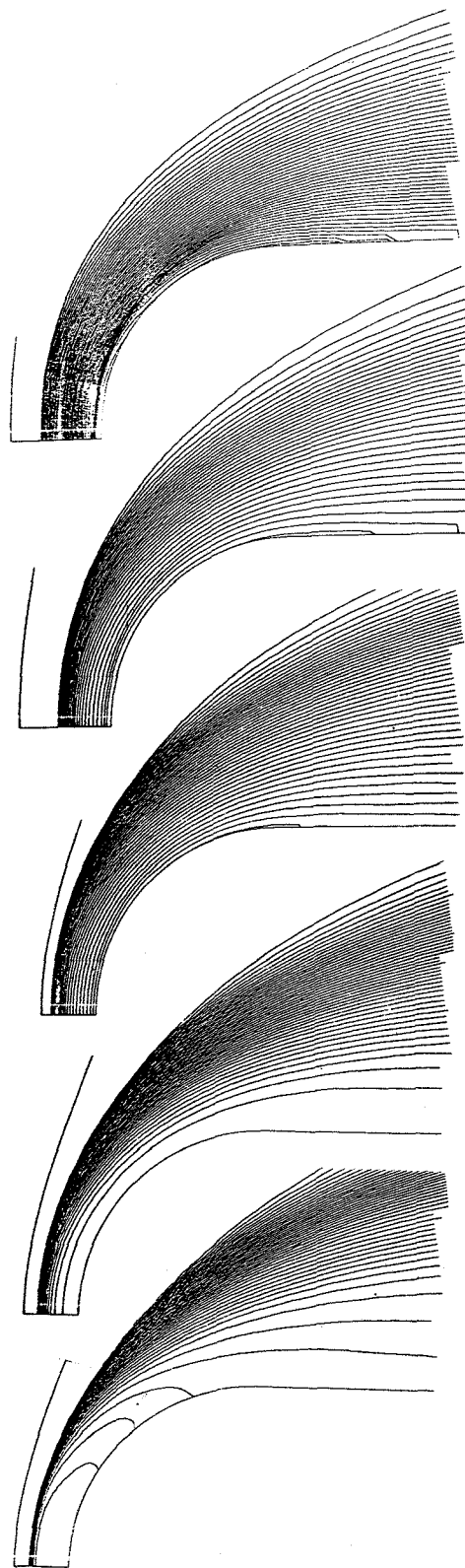

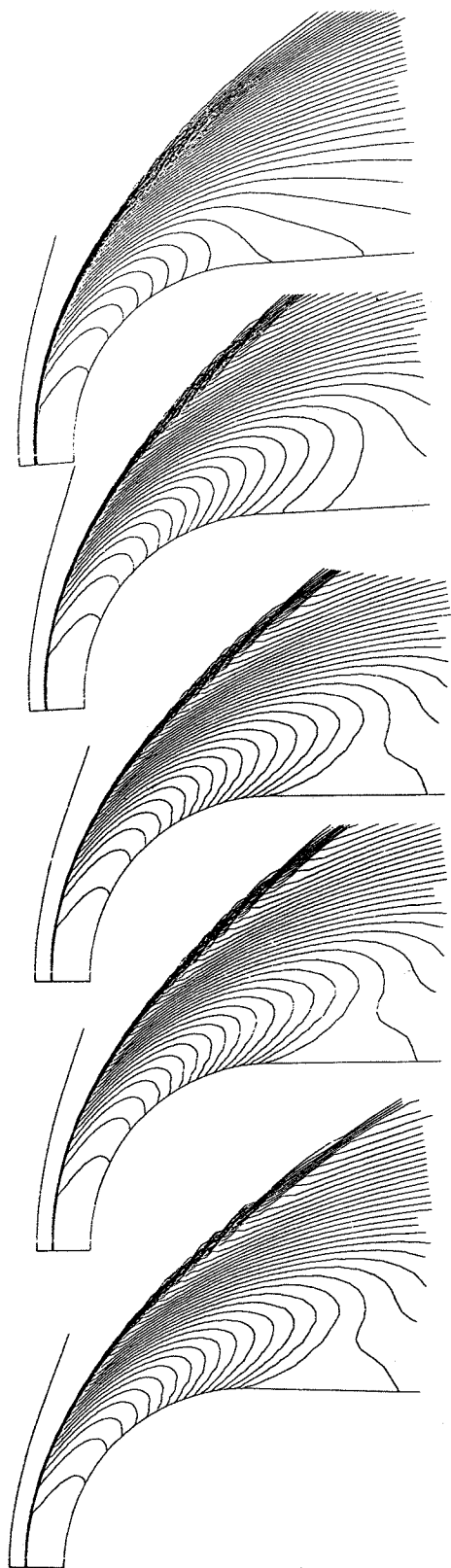Figure 8: O concentration isolines, testcases 2.1 to 2.5

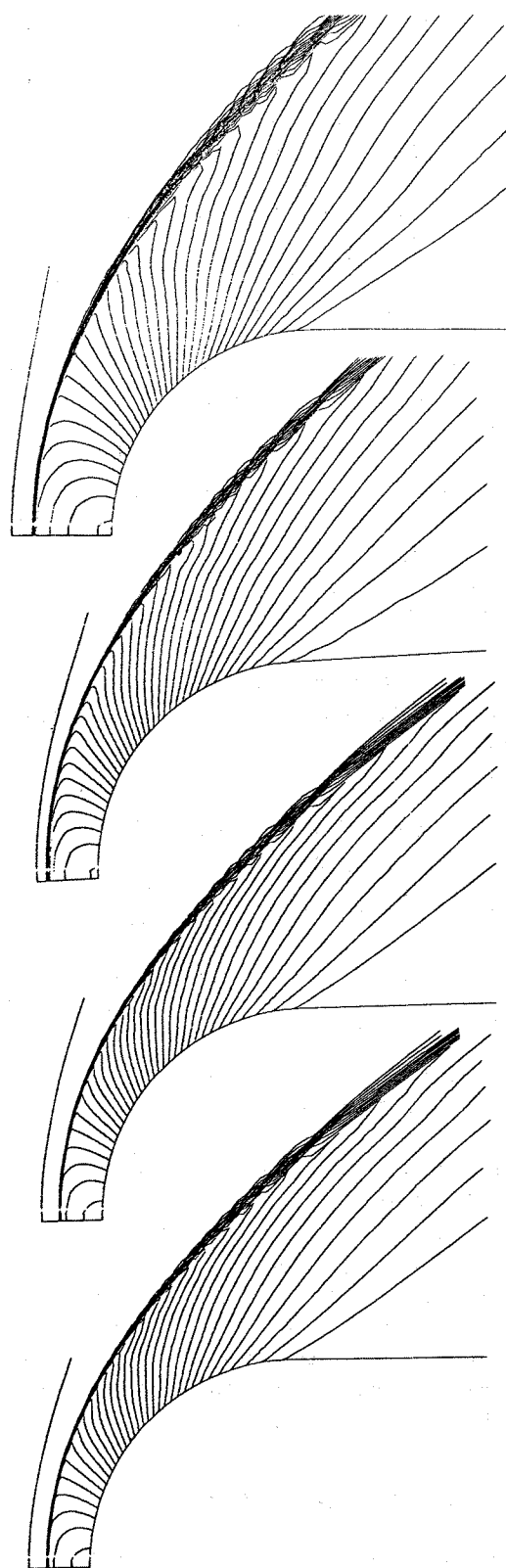Figure 9: O concentration isolines, testcases 2.6 to 2.10

Figure 10: Pressure isolines, (a) testcase 2.0, (b) testcase 2.3, (c) testcase 2.9, (d) testcase 2.11

evolution.

It is interesting to observe that testcase 2.10 was the last that it was possible to run, and that the last cases required an increase in the number of steps through which the chemical reactions introduction was to be relaxed. This supports the statement made in the previous subsection, namely that LUSKE does not reach actual equilibrium but just approaches it much more closely than other methods.

In order to state the performance of the method under the standpoint of efficiency, testcase 2.6 was run also with a previous generation time integration scheme. The comparison scheme employs a simple forward Euler scheme for the fluid dynamics section and the chemical convection terms, and an implicit time discretization of the source terms. It is therefore to be classified as a half-implicit method. This methods does not allow Jacobian freezing, so that, for the sake of completeness, the case was run also with LUSKE and unfrozen Jacobians. Efficiency results of the three runs are presented in table 3. Remark that the advantage of Jacobian freezing is not much evident; this happens because the present testcase required unfrozen Jacobians up to quite a large number of iterations. Though, the advantage of LUSKE over the previuos method remains impressive.

Integration procedure	Steps	Mean CPU per step	CPU time	Time ratios
Half implicit	26949	1.35	36381	1
LUSKE w/o freezing	3356	1.675	5621	.1545
LUSKE (frozen)	3356	1.38	4635	.128

Table 3: Comparisons for test case 2.6: steps and CPU time required for reaching convergence level -1.5

For comparison, fig. 11 presents the O concentration maps for the two schemes, and fig 12 shows the convergence histories in the three cases of table 3 (the two LUSKE runs are indistinguishable).

In conclusion, it is important to remark that the half-implicit method was also tested on other testcases, but showed to be not able to compute testcases from case 2.7, which underlines once more the efficacy improvement offered by LUSKE scheme.

5 Conclusions

A novel scheme for chemically and vibrationally active flows was developed. Testing of this scheme showed excellent behavior regarding both efficiency and efficacy. The 2D code implementing this scheme is intended to be used for computations on double ellipses to build up a better understanding of complex hypersonic phenomena, and extended so as to include lami-
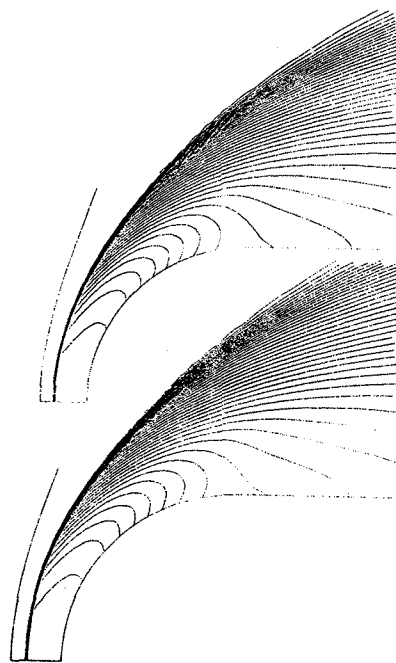

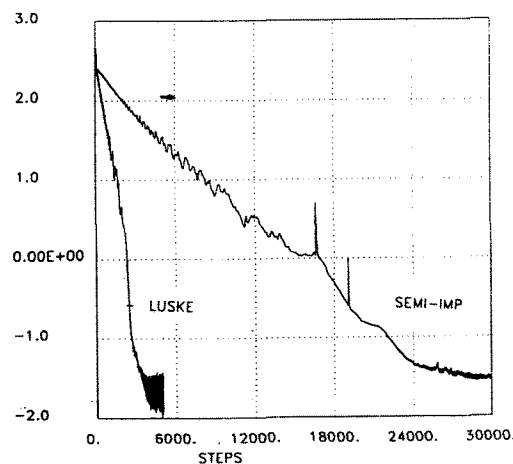Figure 11: O concentration isolines, testcase 2.6, (a) half-implicit method, (b) LUSKE scheme

Figure 12: Convergence histories, testcase 2.6, half-implicit method versus LUSKE scheme

nar viscosity effects. Further extensions of the scheme could eventually lead to cheap computations of fully three-dimensional active flows.

Acknowledgements

References

[1] D. D'Ambrosio. *Flussi Ipersonici: Modelli di non Equilibrio e Previsione Numerica*. Tesi di laurea, Politecnico di Torino, Torino, 1992.

[2] D. D'Ambrosio and M. Pandolfi. *Hypersonic Flows in Thermal and Chemical Nonequilibrium: Comparison between Different Vibration-Chemistry-Vibration Models*. In *Proceedings of the 5th International Symposium on Computational Fluid Dynamics*, volume I, Tokyo, 1993. Japan Society of Computational Fluid Dynamics.

[3] B. Grossman and P. Cinnella. *Flux-split algorithms for flows with non-equilibrium chemistry and vibrational relaxation*. ICAM Report 88-08-03, Virginia Polytechnic Institute and State University, Blacksburg, Va., 1988.

[4] A. Jameson and S. Yoon. *Lower-Upper Implicit Schemes with Multiple Grids for the Euler Equations*. AIAA journal, 25(7):929–935, 1987.

[5] P. Lardy. *Investigation of upwind space discretization for the Navier-Stokes equations. Application to conical supersonic and hypersonic flows*. Project Report 1989-27, von Karman Institute, Bruxelles, 1989.

[6] C. Park. *On Convergence of Computation of Chemically Reacting Flows*. In *AIAA 23rd Aerospace Sciences Meeting*, Reno, Ne, 1985.

[7] C. Park. Nonequilibrium Hypersonic Aerothermodynamics. John Wiley & Sons, New York, 1990.

[8] M. V. Salvetti. *Modelisation Numerique et Physique de Couches de Choc en Regime Hypersonique* . PhD thesis, Universite de Nice-Sophia-Antipolis, Nice, France, 1993.

[9] R. Schrike. *Solution of the conical Euler equations*. Project Report 1988-13, von Karman Institute, Bruxelles, 1988.

[10] P. G. Spazzini. *Improvement and Acceleration of a Conical Solver and Applications to Super/Hypersonic Flows*. Project Report 1992-25, von Karman Institute, Bruxelles, 1992.

[11] S. Yoon and A. Jameson. *An LU-SSOR Scheme for the Euler and Navier-Stokes Equations*. NASA Contractor Report 179556, Lewis Research Center, Princeton, N.J., 1986.